Front. Environ. Sci. Eng. 2022, 16(7): 92
https://doi.org/10.1007/s11783-021-1500-9

RESEARCH ARTICLE

Potassium carbonate-based ternary transition temperature mixture (deep eutectic analogues) for CO_2 absorption: Characterizations and DFT analysis

Hosein Ghaedi[1], Payam Kalhor[2], Ming Zhao (✉)[1], Peter T. Clough[3], Edward J. Anthony[3], Paul S. Fennell[4]

1 School of Environment, Tsinghua University, Beijing 100084, China
2 Department of Chemistry, Tsinghua University, Beijing 100084, China
3 Energy and Power Theme, Cranfield University, Cranfield, Bedfordshire, MK43 0AL, UK
4 Department of Chemical Engineering, Imperial College London, South Kensington, London, SW7 2AZ, UK

HIGHLIGHTS

- Addition of hindered amine increased thermal stability and viscosity of TTTM.
- Addition of hindered amine improved the CO_2 absorption performance of TTTM.
- Good the CO_2 absorption of recycled solvents after two regenerations.
- Important role of amine group in CO_2 absorption of TTTM confirmed by DFT analysis.

GRAPHIC ABSTRACT

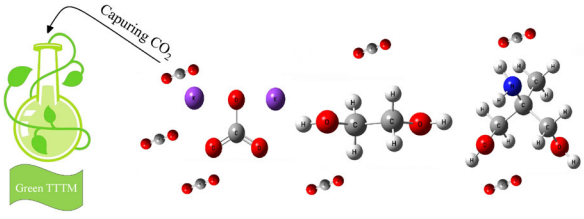

ARTICLE INFO

Article history:
Received 27 May 2021
Revised 8 September 2021
Accepted 7 October 2021
Available online 22 November 2021

Keywords:
Ternary transition-temperature mixture
FT-IR and thermal stability analysis
Viscosity and correlation study
Eyring's absolute rate theory
CO_2 solubility
Density functional theory (DFT)

ABSTRACT

Is it possible to improve CO_2 solubility in potassium carbonate (K_2CO_3)-based transition temperature mixtures (TTMs)? To assess this possibility, a ternary transition-temperature mixture (TTTM) was prepared by using a hindered amine, 2-amino-2-methyl-1,3-propanediol (AMPD). Fourier transform infrared spectroscopy (FT-IR) was employed to detect the functional groups including hydroxyl, amine, carbonate ion, and aliphatic functional groups in the prepared solvents. From thermogravimetric analysis (TGA), it was found that the addition of AMPD to the binary mixture can increase the thermal stability of TTTM. The viscosity findings showed that TTTM has a higher viscosity than TTM while their difference was decreased by increasing temperature. In addition, Eyring's absolute rate theory was used to compute the activation parameters (ΔG^*, ΔH^*, and ΔS^*). The CO_2 solubility in liquids was measured at a temperature of 303.15 K and pressures up to 1.8 MPa. The results disclosed that the CO_2 solubility of TTTM was improved by the addition of AMPD. At the pressure of about 1.8 MPa, the CO_2 mole fractions of TTM and TTTM were 0.1697 and 0.2022, respectively. To confirm the experimental data, density functional theory (DFT) was employed. From the DFT analysis, it was found that the TTTM + CO_2 system has higher interaction energy ($|\Delta E|$) than the TTM + CO_2 system indicating the higher CO_2 affinity of the former system. This study might help scientists to better understand and to improve CO_2 solubility in these types of solvents by choosing a suitable amine as HBD and finding the best combination of HBA and HBD.

1 Introduction

CO_2 is the primary gas and the best-known greenhouse gas (GHG) contributing to global warming. Non-renewable fossil fuel energies are the primary energy sources. Annually, 24 billion tons of CO_2 is produced by human activity, and especially fossil fuel combustion, thus, the primary source of CO_2 emission is fossil fuel including coal, oil, and natural gas which accounts for 65% (United States Environmental Protection Agency, 2014). The CO_2 level in the atmosphere has raisen from 310 ppm in 1958 to 413.71 ppm in 2021 (August 24) according to the latest reading reported by Scripps Institution of Oceanography (2021), and is rising faster and faster; that is why contemporary research has focused on ways to slow or stop this trend and globally, there has been a significant increase in interest in reducing CO_2 emissions in both

✉ Corresponding author
E-mail: ming.zhao@tsinghua.edu.cn

academics and industry, notably in China. It is anticipated that the CO_2 concentration will reach 900-1100 ppm if we will not take immediate and major actions to reduce the CO_2 emissions (Wang and Song, 2020) and the temperature will rise 5°C by the century's end (Pachauri and Reisinger, 2007). As a result, it is necessary to reduce CO_2 emissions from stationeries especially fossil fuel power plants. Bearing in mind that fossil fuels will continue to be the dominant energy resource in the next decades, carbon capture utilization, and storage (CCUS) is essential and the most promising technology to mitigate these problems (Ghaedi et al., 2017d; Hu et al., 2018; Nawar et al., 2019). CCUS is a method of capturing CO_2 emissions from big industrial facilities including coal, oil, and natural gas combustion plants, as well as other industrial processes, before they are released into the atmosphere. Pre- or post-combustion, oxyfuel, and electrochemical separation are all part of this technique. Even though each of these approaches has its own set of benefits and drawbacks, post-combustion is the most basic CCUS technology for CO_2 capture. The post-combustion capture process using solvents is a mature technology for CCUS. The absorption process using aqueous amine solutions is an efficient method for capturing CO_2 (Xie et al., 2014). However, there are several concerns over amine solvents for post-combustion CO_2 capture, for example, high energy required for solvent regeneration, corrosion problems, amine volatility, and the environmental and health impact due to the degradation products of amine solvents. As a result, scientists are attempting to find alternate solvents to amines; hence, solvent development is the central part of improving post-combustion CCUS technologies.

The use of ionic liquids (ILs) and deep eutectic solvents (DESs) has grown in popularity during the last two decades, both industrially and scientifically. Despite many unique properties, high cost, complex reaction steps, high viscosity, potential toxicity, limited biodegradability, required purification, and energy-intensive of regeneration steps are the main disadvantages associated with IL limiting their application at a large scale (Chemat et al., 2016; Kalhor et al., 2021). DESs and transition-temperature mixtures (TTMs) (deep eutectic analogs) have emerged as possible alternatives to ILs and traditional solvents. They are receiving increasing attention for many purposes, but in particular, capturing CO_2. These new solvents have many of the same properties as ILs and, however, they are more advantageous due to the potential low cost of initial components, easy preparation procedure, non-toxic, non-volatility, less corrosive, biodegradability, no further purification, high thermal stability, and electrical conductivity (Ghaedi et al., 2017a; Ghaedi et al., 2017b; Ghaedi et al., 2017 g; Xu et al., 2016). It is worth noting that the main difference between DES and TTM solvents is that the DSC curve of DES shows a melting or freezing temperature, however, TTM has only the glass transition temperature in the DSC curve (Ghaedi et al., 2018b; Mat Hussin et al., 2020). On the other hand, still there is a debate between researchers in order to categorize these new solvents. It was stated that for some ILs and DESs which are not non-easily crystallizable even the melting or freezing temperature is not observed; then, they can be named as DESs (Jiang et al., 2020; López-Salas et al., 2014a; López-Salas et al., 2014b). Other research groups have reported similar results (Guo et al., 2013; Gutierrez et al., 2011; Morrison et al., 2009).

According to the appropriate safety data sheet (SDS), AMPD is non-toxic to fish on an acute basis ($LC_{50}>100$ mg/L) and is not likely to accumulate in the food chain (bio-concentration potential is low). Due to very low (but observable) volatility, exposure to vapor is minimal and it may evaporate slowly from products containing it. It also has low toxicity if swallowed. AMPD is unlikely to persist in the environment and is ultimately biodegradable, which suggests it will be removed from soil and water environments, including biological wastewater treatment plants. Also, regarding ecotoxicology, persistence, and bioaccumulation, K_2CO_3, EG, and AMPD are not suspected of being environmental toxins and bioaccumulative according to Environment Canada's Domestic Substance List. It has been reported that the toxicities of DESs are lower than their components (Wen et al., 2015).

Potassium carbonate (K_2CO_3) is used in large amounts in industry and consumer products. K_2CO_3 is environmentally benign, non-toxic, and is not carcinogenic or genotoxic. The only possible potential hazard of K_2CO_3 to the aquatic environment is caused by a raised alkalinity due to the carbonate ion (pH buffering effect). Of particular significance is the fact that the K_2CO_3 solution process is an important technology for CO_2 removal and has been used in many plants around the world because of several advantages: easy regeneration, inexpensive solvent, low toxicity, and low tendency to degrade (Borhani et al., 2015).

Ethylene glycol (EG) is an odorless, colorless, sweet, relatively nonvolatile, and slightly viscous organic liquid, used as a raw chemical in the production of a large number of products such as polyester fibers for clothes and many industrial and commercial applications, for example, antifreeze and coolant. EG is not persistent in soil, and surface/groundwater, and air. According to the acute toxicity data, EG does not bioaccumulate in and is practically non-toxic to aquatic organisms. (Hayyan et al., 2013) used EG as an HBD of DES-based choline chloride and investigated the toxicity using Gram-positive and Gram-negative bacteria. According to the results, the tested DES did not have a toxic effect toward the studied bacteria. Therefore, the toxicity of the final mixtures of K_2CO_3, EG, and AMPD is likely to be lower than that of their original components.

The Fourier transform infrared spectroscopy (FT-IR) analysis is commonly applied to examine the interactions between various groups and to analyze and identify the

structure of materials. It is particularly useful for determining the hydrogen bond strengths between components of TTMs or TTTMs. It is essential to do a thermogravimetric analysis (TGA) of the solvents used for CO_2 absorption. To be effective, the solvent employed for CO_2 absorption must be thermally stable at the studied absorption temperature. Furthermore, in order to develop new TTMs with enhanced functionality, a better understanding of CO_2 absorption utilizing TTMs is required. Computational chemistry approaches namely Density Functional Methods (DFT) can be applied to understand the mechanism of CO_2 and TTM-molecule interaction. DFT simulation is an excellent approach to get molecular structure-property relationships, which might help researchers for developing novel task-specific TTMs for better CO_2 capture.

As a result, the primary goals of this study are to (1) analyze the structure and thermal stability of prepared samples, (2) measure the viscosity of prepared samples, (3) measure the CO_2 solubility in the fresh and reused potassium carbonate-based TTM or TTTM, and (4) study CO_2-capturing mechanism using DFT simulation.

2 Materials and methods

2.1 Chemicals

K_2CO_3 and AMPD were purchased from Sigma-Aldrich. EG was supplied by *R&M* Chemicals. The details of pure chemicals are presented in Table 1. Fig. S1 shows the chemical structure of individual compounds.

2.2 Preparation of solvents

Binary TTM was prepared in the molar ratio of 1:10 for K_2CO_3 to EG at a temperature of about 353 K for 1–2 h. To prepare TTTM, the hindered amine AMPD was mixed with the binary mixture in a molar ratio of 1:10:1 for K_2CO_3-EG-AMPD. The AMPD was added into the binary mixture of K_2CO_3 and EG after about 30 min. After 1 h continues stirring at the same temperature, a liquid was obtained. All solvents were kept in a closed vial to prevent contamination with moisture or any other contaminants for further use without purification. More details of solvents are shown in Table 2.

2.3 Characterization

FT-IR spectrometer (Thermo Scientific™ Nicolet™ iS 10) was applied to record infrared spectra of all materials in the region of 4000 cm^{-1} to 400 cm^{-1}. A thermogravimetric-differential thermal analysis-mass spectrometry (TG-DTA-MS) instrument (Rigaku, Smart loader) was employed for the thermal stability analysis of samples at a temperature range from 300 K to 800 K at a heating rate of 10 K/min under Helium atmosphere with a flow rate of 100 mL/min. A digital rolling ball micro-viscometer (Anton Par, model Lovis-2000M/ME) was employed to measure the viscosity of liquids from 293.15 K to 333.15 K.

2.4 CO_2 solubility and solvent regeneration experiments

Using a high-pressure solubility cell (SOLTEQ BP-22) (see Fig. S2), the pressure drop was utilized to test CO_2 solubility in solvents. A set of equations was used to calculate the amount of CO_2 absorbed as stated in Section 1 of the supplementary material (Ghaedi et al., 2017d). For the regeneration study, the prepared solvents were collected after CO_2 solubility measurements. The recycling of solvents was conducted by desorbing CO_2 via the application of depressurization and vacuum (< 45 kPa). The collected samples were placed in a vacuum oven for assuring the full CO_2 removal for 24 h. Following that, the

Table 1 Description of materials used for the synthesis of TTM and TTTM.

Chemical name	CAS number	Supplier	Purity	Melting point	Purity analysis
Potassium carbonate	584-08-7	Sigma-Aldrich	> 99.90	891 °C [a]	Trace metals analysis
2-amino-2methyl-1,3-propanediol	115-69-5	Sigma-Aldrich	> 99.00	109–111 °C [a]	Titration with $HClO_4$
Ethylene glycol	107-21-1	*R & M* Chemicals	> 99.50	–13.0 °C [a]	Gas chromatography

a) This information was obtained from the safety data sheet (SDS).

Table 2 The details of prepared TTM and TTTM

Solvent		HBA		HBD		Molar ratio		Water content (mass fraction) [e]	Glass transition, T_g (°C) [f]
Symbol	$M_{TTM/TTTM}$ [a]	Symbol	M_{HBA} [b]	Symbol	M_{HBD} [c]	HBA	HBD		
TTM	68.992	K_2CO_3	138.21	EG	62.07	1	10	0.0060	–121.5
TTTM	72.004	K_2CO_3	138.21	EG & AMPD	62.07 105.14	1	10:1[d]	0.0068	–83.3

[a] $M_{TTM/TTTM}$ molecular weight of TTM or TTTM in g/mol.
[b] Molecular weight of HBA in g/mol.
[c] Molecular weight of HBD in g/mol.
[d] (10) is the molar ratio of EG and (1) is the molar ratio of AMPD.
[e,f] Water content and glass-transition temperature of samples were taken from previous work (Ghaedi et al., 2018b).

collected solvents were tested for CO_2 solubility to determine their possible application for recycling.

2.5 Density functional theory (DFT)

DFT is a useful tool to simulate and gain information about molecular structure-property relationships; and the CO_2-capturing mechanism, helping researchers to develop and synthesize new task-specific solvents for CO_2 capture (Altamash et al., 2016). Therefore, the geometry optimizations were performed using DFT with Becke three-parameter (Exchange), Lee, Yang, and Parr correlation (B3LYP) and basis set of 6-31 + G (d, p) which is widely used in computational studies (Yang et al., 2021; Khan et al., 2020). B3LYP was selected for all calculations due to its remarkable performance over a wide range of systems. To do the calculations and optimizations, the GAUSSIAN 09 software package with the aid of the Gauss View visualization program was used in this study. The initial geometries for each solvent and CO_2 + solvent were generated using previously optimized geometries of K_2CO_3, EG, AMPD, and free CO_2 developed using the Gauss View software. The standard counterpoise method was used to correct the absolute interaction energy (ΔE) to avoid basis set superposition error (BSSE) for the systems containing two or more molecules (Altamash et al., 2016).

3 Results and discussion

3.1 FT-IR analysis

For prepared solvents such as TTMs, identifying and studying the functional groups, investigation of the chemical bonds, the combinations of various components, and the observed changes in their structure are the important aspects. Infrared spectroscopy is beneficial and useful not only for the identification of molecules and studying their structure but also in studying the interactions which have a great effect on molecular vibrations. Figs. S3, S4, and S5 show the FT-IR spectroscopy of the single components including K_2CO_3, EG, and AMPD. The FT-IR spectra of TTM and TTTM are displayed in Figs. 1 and 2, respectively.

3.1.1 Hydroxyl functional group (OH)

From Figs. 1 and 2, the OH stretching vibrations which are mostly affected by hydrogen bonding occurred in the region of 3800–3100 cm^{-1}. The OH stretching bands in the condensed phase are observed at a wavenumber range of 3550 cm^{-1}–3230 cm^{-1}, for example, these bands are generally centered at 3400 cm^{-1} for water, alcohols, and phenols (Larkin, 2011). Therefore, the broadening and

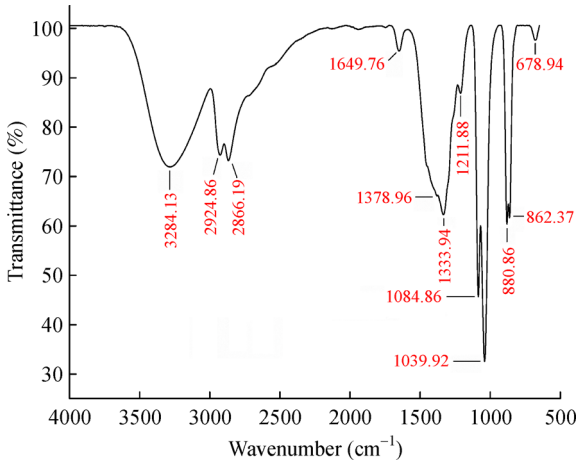

Fig. 1 The spectrum of TTM.

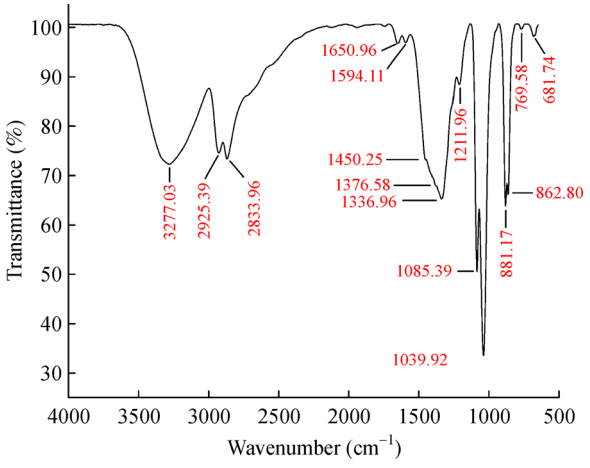

Fig. 2 The spectrum of TTTM.

shifting of OH stretching vibrations indicate the hydrogen-bond formation. From Figs. 1 and S4, it is clear that the absorption band at 3285.44 cm^{-1} in pure EG changed to a marginally broader and stronger band at the wavenumber of 3284.13 cm^{-1} after the formation of TTM. Pure AMPD (see Fig. S4) reveals broadband at 3245.78 cm^{-1} assigned to the υ(OH) band which is stronger than that of pure EG. From Fig. 2, the OH stretching vibration in TTTM reveals a band at 3277.03 cm^{-1}, approximately similar to TTM. Also, it is obvious from Figs. 1 and 2 that the intensities of different absorption bands of both solvents are almost the same. Then, it can be stated that the hydrogen bonds are strong in this region. Generally, peaks observed in the 900–500 cm^{-1} region are the OH and NH_2 wagging vibrations (Larkin, 2011). In the TTM, TTTM, and pure EG, there are two positive peaks at wavenumbers between 850 cm^{-1} and 870 cm^{-1} indicating the OH wagging vibrations. In pure AMPD, Peaks at 914.84 cm^{-1} and 886.29 cm^{-1} can be possibly attributed to these vibrations.

3.1.2 Amine functional group (–NH_2)

AMPD is considered a primary amine, with an amino group –NH_2. Usually, primary amines give two weak absorptions in the -NH_2 stretching bands region between 3400 cm^{-1} and 3100 cm^{-1} including the out-of-phase and in-phase NH_2 stretching vibrations. Normally, out-of-phase NH_2 stretching bands are weaker in the spectra than the in-phase NH_2 stretching bands. The out-of-phase NH_2 stretching band is considered as an antisymmetric vibration and the in-phase NH_2 stretching band is regarded as the symmetric vibration in the spectra. According to Fig. S4, three peaks appeared in this region. The peak at 3327.84 cm^{-1} is ascribed to the antisymmetric –NH_2 vibration. Regarding the in-phase –NH_2 stretching bands, it is difficult to interpret this peak in the spectra. One may consider the peak at a wavenumber of 3188.92 cm^{-1} as in-phase –NH_2 stretching bands. It is a moot point and may not be true due to the fact that –NH_2 bands are weaker than OH bands, and, thus, –NH_2 bands have a higher frequency. Moreover, it is well established that in amines, a low-intensity shoulder occurs at the wavenumber around 3200 cm^{-1} (Larkin, 2011). Indeed, an overtone of the N-H bending vibration at a wavenumber of 1617.01 cm^{-1} caused this low-intensity band at the wavenumber of 3188.92 cm^{-1} in pure AMPD. It should be mentioned that it is more complex to analyze the curve affected by overlapping bands. Therefore, the peak at a wavenumber of 3188.92 cm^{-1} does not indicate the in-phase-NH_2 stretching band and, in fact, this band has been overlapped by OH stretching bands and cannot be observed in the spectra. From Fig. 2, it is quite clear that in the prepared TTTM, the OH stretching bands overlapped the in-phase –NH_2 stretching bands. The peaks at the wavenumbers of 1640 cm^{-1} to 1560 cm^{-1} are associated with the N-H bending modes (scissoring) with medium to strong intensity bands (Larkin, 2011). In pure AMPD, this mode appeared at 1617.01 cm^{-1}. As mentioned earlier, an overtone of this mode caused a band at 3039.96 cm^{-1} and after the formed TTTM, it was possibly shifted to a lower intensity band at the wavenumber of 1594.11 cm^{-1} (see Fig. 2). As shown in Fig. 1, this peak cannot be present in the spectra of TTM due to the absence of NH_2 groups in its structure. The NH_2 wagging vibrations in TTTM and pure AMPD occurred at the wavenumbers of 769.58 cm^{-1} and 776.70 cm^{-1}, respectively. These peaks were absent in the spectra of TTM and pure EG.

3.1.3 The aliphatic (-CH_n) vibrational modes

The region between 3000 and 2700 cm^{-1} mainly contains the peaks of aliphatic stretching vibrations. Normally, the CH_2 stretching vibrations appear at 2940–2915 cm^{-1} and 2870–2840 cm^{-1}, while bands for CH_3 stretching vibrations occur at wavenumbers of 2975–2950 cm^{-1} and 2885–2865 cm^{-1}. Since these bands are not strong, they may not be distinguishable in the spectrum (Larkin, 2011). Here, the C-H stretching vibrations include methylene (CH_2 antisymmetric and symmetric stretching) and methyl (CH_3 symmetric stretching). According to Fig. S1, there is no CH_3 group on the structure of pure EG and, hence, there are no CH_3 stretching vibrations. For this case, the region of CH_2 stretching vibrations was between two vicinities of 2935.41 cm^{-1} and 2873.18 cm^{-1} accompanied by two positive peaks and the same intensity. In pure AMPD, the CH_3 symmetric stretching out of phase occurred at 2972.80 cm^{-1} and CH_2 stretching vibration was observed at 2960.90 cm^{-1}. The in-phase CH_2 stretching vibrations were observed between 2905.92 cm^{-1} and 2752.86 cm^{-1}.

As illustrated in Fig. S4, there is a low-intensity peak at 3039.96 cm^{-1} for pure AMPD which may not be an indication of the aliphatic stretching vibrations, because the aliphatic stretching vibrations are sharp and spiky. In all probability, this can be attributed to an overtone of the 1500.07 cm^{-1} owing to Fermi resonance between the methylene CH_2 stretching vibrations. As seen from Figs. 1 and 2, these aliphatic stretching vibrations were seen at the wavenumbers of 2924.86 cm^{-1} (as CH_3 stretching vibration) and 2866.19 cm^{-1} (as CH_2 stretching vibration) for TTM and at the wavenumbers of 2925.39 cm^{-1} (as CH_3 stretching vibration) and 2866.96 cm^{-1} (as CH_3 stretching vibration) for TTTM along with two positive peaks and the same intensity. Further explanations on other vibrations are available in the Supplementary Material.

3.2 TGA results

An effective solvent for CO_2 absorption should have high thermal stability at absorption temperatures. To date, TGA data on TTMs/TTTMs are inadequate; and, there is a need to collect TGA data of these solvents. Therefore, the thermal stabilities of TTM and TTTM were analyzed in this study. Fig. 3 (a) illustrates the TGA curves of pure components and TGA-DTA (differential thermal analysis) curves of prepared solvents are shown in Fig. 3 (b). There are two decomposition steps in these curves, as seen in Fig. 3 (b). The thermal decomposition temperature of salts is greater than that of HBDs (Abbas and Binder, 2010). As a result, the first and second decomposition steps reflect the temperature at which HBDs and salt decompose, respectively. The first decomposition temperatures for TTM and TTTM occurred at about 383 K and 389 K, respectively. As seen in Fig. 3 (b), the second weight loss was accompanied by endothermic peaks at 414 K and 457 K for TTM and TTM, respectively. The DTA curves shifted upward after the second decomposition which is attributed to the mass loss. Moreover, TTTM is slightly more stable than TTM. As seen in Fig. 3, AMPD is more stable than EG. Therefore, the addition of AMPD enhanced the thermal stability of TTTM. In the previous work, the result disclosed that the viscosity of the solvent affects its thermal stability (Ghaedi et al., 2018a; Ghaedi et al., 2017c). The

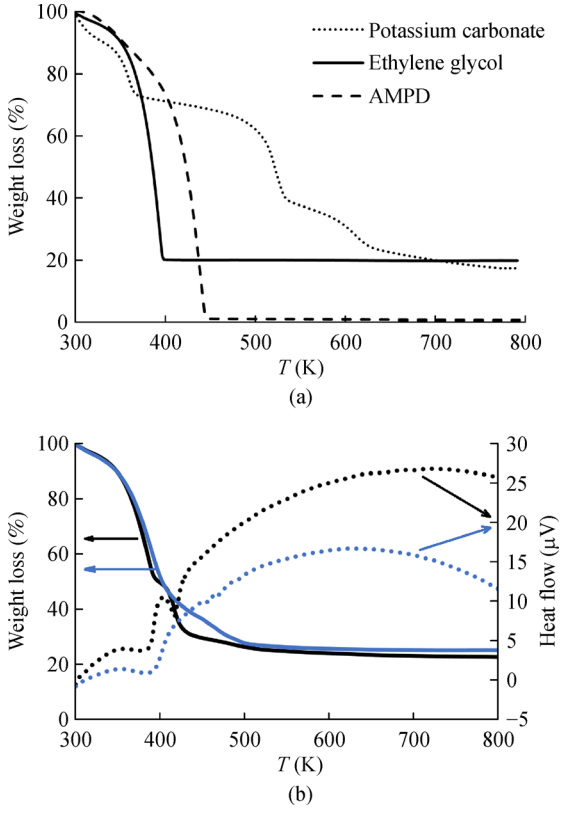

Fig. 3 (a) TGA curves for pure components and (b) TGA-DTA curves of prepared solvents from 300 K to 800 K at the heating rate of 10 K/min under Helium atmosphere with a flow rate of 100 mL/min. The black solid and dashed lines represent the TGA and DTA curves of TTM, respectively. The blue solid and dotted lines represent the TGA and DTA curves of TTTM, respectively.

hydrogen-bonding interactions have an effect on the thermal stability of solvents. Higher OH stretching frequencies indicate weaker hydrogen bonds inside the solvents. From the FT-IR results, the OH stretching wavenumber in TTTM was lower than in TTM. This is an indication of the strong hydrogen bonding in TTTM resulting in its higher thermal stability. Another possible reason could be that the structure of TTTM has is a longer alkyl chain length due to AMPD resulting in higher thermal stability. Previously, a similar finding was reported (Ghaedi et al., 2018a; Ghaedi et al., 2017c).

3.3 Viscosity results

Table S1 lists the experimental viscosity data of pure EG, TTM, and TTTM. The temperature dependence of experimental viscosity values of pure EG, TTM, and TTTM is shown in Fig. 4. Table S2 compares the viscosity of EG in our study to that found in the literature (Yang et al., 2003). As presented in Table S2, there was a good agreement between experimental and literature data with a low average absolute deviation (*%AAD*) of 0.3358.

By raising the temperature, the viscosity of solvents and

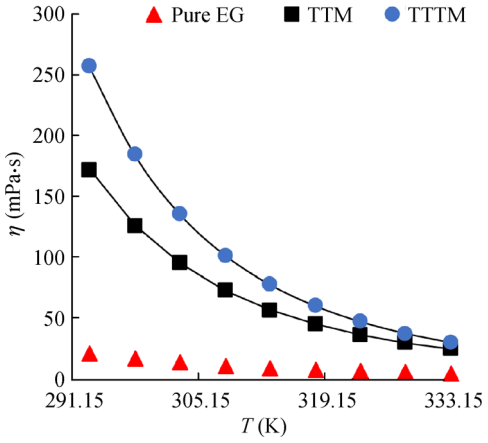

Fig. 4 Experimental viscosity (η) of pure EG, TTM, and TTTM at several temperatures. The solid lines show the viscosity data obtained by Eq. (1).

EG decreased. The higher viscosity of solvents is directly associated with their intermolecular interactions. Thus, the higher temperature decreases the internal resistance of molecules and their intensity accordingly, and they are less viscous and flow more easily. It is seen from Fig. 4 that both TTM and TTTM had a higher viscosity than EG. Moreover, the viscosity of TTTM increased over the temperature range by the addition of AMPD. For instance, the viscosity of TTTM was 184.93 mPa·s, higher than that of TTM (126.07 mPa·s) at 298.15 K. To correlate the experimental viscosity data an empirical relation was used as given below (Ghaedi et al., 2018a; Ghaedi et al., 2017f; Ghaedi et al., 2018b):

$$\ln\left[\frac{\eta}{(\rho \times M)_{\mathrm{TTM/TTTM}}}\right] = A_0 + \frac{A_1}{T} + \frac{A_2}{T^2} + \ldots + \frac{A_n}{T^n} = \sum_{i=0}^{n} \frac{A_i}{T^i}, \quad (1)$$

where T is the temperature; and ρ is the density (available in previous work (Ghaedi et al., 2018b)); A_i is the fitting parameter, and $M_{\mathrm{TTM/TTTM}}$ is the molecular mass of TTM or TTTM in g/mol.

Additionally, several relations were used for the correlation study, for example, Arrhenius, Seddon, Andrade, Vogel-Fulcher-Tammann (VTF), Waterton, and Yaws, as mentioned in the Supplementary Material. As evident in Table S3 and Fig. 4, a quite low *RMSE* value between the experimental and the calculated data from Eq. (1) shows that the suggested correlation appropriately describes the viscosity of solvents as a function of temperature, density and molecular weight of solvents; hence, Eq. (1) can be used in the calculation of viscosity with high accuracy. The activation energy (E_a, J/mol) of solvents can be estimated from experimental viscosity. A

higher E_a value indicates that the ions cannot easily move past each other due to a highly viscous fluid. From the data presented in Table S3, the E_a values of TTTM estimated by the Arrhenius and Seddon relations are higher than those for TTM indicating that TTTM is more viscous. Further, Eq. (2) was used for calculating the E_a as a function of temperature, as given below (Ghaedi et al., 2017f):

$$E_a = R \times \frac{\partial\left(\ln[\eta(T)]\right)}{\partial(1/T)} = R \times \left(A_1 + \frac{2 \times A_2}{T} + \frac{3 \times A_3}{T^2}\right), \quad (2)$$

where A_1, A_2, and A_3 are the fitting parameters derived from Eq. (1), as listed in Table S3. Then, these fitting parameters were used to calculate E_a data for TTM and TTTM, as listed in Table S4. Fig. 5 illustrates the E_a against temperature. As demonstrated in Fig. 5, by raising the temperature, the value of E_a decreased moderately. Moreover, TTTM has higher activation energy than TTM indicating higher viscosity of this solvent.

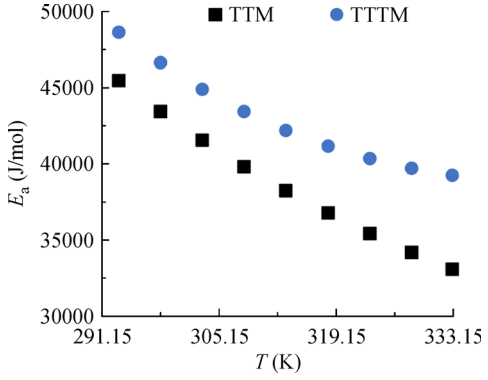

Fig. 5 The E values of TTM and TTTM as a function of T obtained from Eq. (2).

Eyring's absolute rate theory is applied to express the viscosity of a liquid (Ghaedi et al., 2017f):

$$\eta = \frac{h \times N_A}{V} \exp\left(\frac{\Delta G^*}{R \times T}\right), \quad (3)$$

where and T denotes temperature; R signifies the gas constant, V is the molar volume of solvents (available in previous work (Ghaedi et al., 2019)); h is Planck's constant; N_A is Avogadro's number, and ΔG^* represents the molar Gibbs free energy of activation calculated from the following equation:

$$\Delta G^* = \Delta H^* - T \times \Delta S^*. \quad (4)$$

The viscosity of a liquid can be calculated from the following equation by combining Eq. (4) and Eq. (3):

$$R \times \ln\left(\frac{\eta \times V}{h \times N_A}\right) = \frac{\Delta H^*}{T} - \Delta S^*. \quad (5)$$

In the above equations, ΔH^* represents the enthalpy of viscous flow and ΔS^* is the entropy of viscous flow. For some cases, the relationship between $R \cdot \ln(\eta \cdot V/h \cdot N_A)$ and $1/T$ is linear, and the slope is equal to ΔH^* and the intercept is equal to-ΔS^* (Vranes et al., 2012). However, there is some curvature evident by plotting $R \cdot \ln(\eta \cdot V/h \cdot N_A)$ against $1/T$ for some other liquids, as reported in previous work (Ghaedi et al., 2017f). For the solvents studied here, by plotting $R \cdot \ln(\eta \cdot V/h \cdot N_A)$ against $1/T$, as shown in Fig. S6, the values of R^2 were 0.998 and 0.999 for both TTM and TTTM, respectively, indicating the linear relationship. Table 3 lists the ΔG^* values obtained from Eq. (4) used. For the data in Table 3, TTTM has higher ΔG^* values than TTM at the studied temperatures indicating a stronger interaction in TTTM in comparison to TTM. Since the dependence of $R \cdot \ln(\eta \cdot V/h \cdot N_A)$ was a linear function of $1/T$, practically speaking, it may be assumed that ΔH^* is an independent function in this temperature range.

Table 3 The ΔG^* (J/mol) values solvents at the studied temperatures

T (K)	TTM	TTTM
293.15	24428.00	25572.34
298.15	24183.33	25277.27
303.15	23938.66	24982.21
308.15	23693.99	24687.14
313.15	23449.32	24392.08
318.15	23204.65	24097.01
323.15	22959.98	23801.95
328.15	22715.31	23506.88
333.15	22470.64	23211.82

From the data in Table 4, it was found that $T \cdot \Delta S^*$ values are lower than ΔH^* values. It means that the energetic influence (ΔH^*) is significant rather than entropic influence (ΔG^*) (Ghaedi et al., 2017f); then, the interactional factor dominates the structural factor.

Table 4 The ΔH^* and ΔS^* of solvents

Solvent	ΔH^* (J/mol)	ΔS^* (J/(mol·K))	R^2
TTM	38773	48.934	0.998
TTTM	42872	59.013	0.999

3.4 CO_2 solubility and regeneration results

The CO_2 solubility measurements at 303.15 K and pressure up to 1.8 MPa are presented in Table 5. As listed in Table 5, the CO_2 solubility in TTTM was higher than

Table 5 CO_2 solubility in fresh and recycled TTM and TTTM at the temperature of 303.15 K

Fresh		First recycled		Second recycled	
P^E (MPa)	x_{CO_2}	P^E (MPa)	x_{CO_2}	P^E (MPa)	x_{CO_2}
TTM					
1.794	0.1697	1.805	0.1654	1.815	0.1638
1.604	0.1428	1.613	0.1393	1.625	0.1375
1.324	0.1211	1.319	0.1180	1.331	0.1164
1.080	0.1013	1.092	0.0987	1.101	0.0977
TTTM					
1.780	0.2022	1.794	0.1976	1.802	0.1961
1.598	0.1741	1.591	0.1694	1.609	0.1671
1.301	0.1483	1.316	0.1457	1.325	0.1443
1.010	0.1203	0.998	0.1175	1.015	0.1159

that that in TTM. By adding AMPD to the mixture, TTTM has shown a better affinity for absorbing CO_2 in comparison to TTM (without AMPD). It may be reasoned that an additional amino group (–NH_2) in the structure of TTTM improves its CO_2 solubility. In the previous work, it was found that CO_2 solubility in DESs increases as alkyl chain length increases (Ghaedi et al., 2017e). From Fig. S1, it is clear that TTTM containing two HBDs has a longer alkyl chain length than TTM which is composed of only one HBD; consequently, TTTM exhibited a higher CO_2 solubility than TTM. It is worth comparing CO_2 solubility in the studied solvents with other solvents. In the previous work, the CO_2 solubility in phosphonium-based DESs was measured with different HBDs in different molar ratios (Ghaedi et al., 2017e). A comparison shows that CO_2 solubility in TTM and TTTM in this work is lower than that in phosphonium-based DESs. However, the main finding of this research work is that using amine as a third component can improve CO_2 solubility. Due to the tunable properties of DESs and TTMs have, new solvents using different amines as HBDs could be prepared for the CO_2 absorption improvement. Table 5 presents the CO_2 solubility data in recycled TTM and TTTM. The data show that the CO_2 solubility in fresh and recycled TTM and TTTM did not change considerably and that the difference is not significant.

Fig. 6 compares the CO_2 solubility in TTTM and several ILs such as trihexyltetradecylphosphoniump [THTDP]-based IL with anion of bis(trifluoromethyl)sulfonylimide ($[NTf_2]^-$) and imidazolium-based ILs containing different cations and anions. As illustrated in Fig. 6, TTTM, showed a better CO_2 absorption performance than some ILs such as $[C_2mim][EtSO_4]$, $[C_6mim][BF_4]$, and $[C_6mim][BF_4]$. However, the CO_2 solubility in TTTM was less than those of ILs containing $[NTf_2]^-$ anion and a longer alkyl chain length on the cation such as $[THTDP][NTf_2]$, $[C_8mim][NTf_2]$ and $[C_8mim][PF_6]$. From the data presented in Table 6. TTTM exhibited a higher CO_2 absorption in comparison with other TTMs and DESs in the literature.

3.5 DFT analysis

Fig. 7 illustrates the optimized structures of TTM and TTTM before and after interaction with CO_2. The optimized structures of K_2CO_3, EG, AMPD, and free CO_2 are shown in Fig. S7 in Supplementary Material. The following equations were used to compute the ΔE of those processes related to binding energy for K_2CO_3 salt ($\Delta E_{K_2CO_3}$), TTM formation (ΔE_{TTM}), TTTM formation (ΔE_{TTTM}), and CO_2 capture by these two solvents ($\Delta E_{TTM\,+\,CO_2}$) and ($\Delta E_{TTTM\,+\,CO_2}$):

$$\Delta E_{K_2CO_3} = E_{K_2CO_3} - [2 \times E_K + \times E_{CO_3}] \quad (6)$$

$$\Delta E_{TTM} = E_{TTM} - [E_{K_2CO_3} + 10 \times E_{EG}] \quad (7)$$

$$\Delta E_{TTM+CO_2} = E_{TTM+CO_2} - [E_{K_2CO_3} + 10 \times E_{EG} + E_{CO_2}] \quad (8)$$

$$\Delta E_{TTTM} = E_{TTTM} - [E_{K_2CO_3} + 10 \times E_{EG} + E_{AMPD}] \quad (9)$$

$$\Delta E_{TTTM+CO_2} = E_{TTTM+CO_2} - [E_{K_2CO_3} + 10 \times E_{EG} + E_{AMPD} + E_{CO_2}] \quad (10)$$

where $E_{K_2CO_3}$, $E_{TTM\,+\,CO_2}$, and $E_{TTTM\,+\,CO_2}$ represent the (counterpoise corrected) energies of $E_{K_2CO_3}$, TTM + CO_2, and TTTM + CO_2, respectively. E_{EG}, E_{AMPD}, and E_{CO_2} correspond to the energies of K_2CO_3, EG, AMPD, and free CO_2, respectively. (García et al., 2015) calculated the $|\Delta E|$ for processes related to CO_2 absorption using choline chloride- malonic acid and choline chloride-glycerol and stated that choline chloride- malonic acid exhibited better

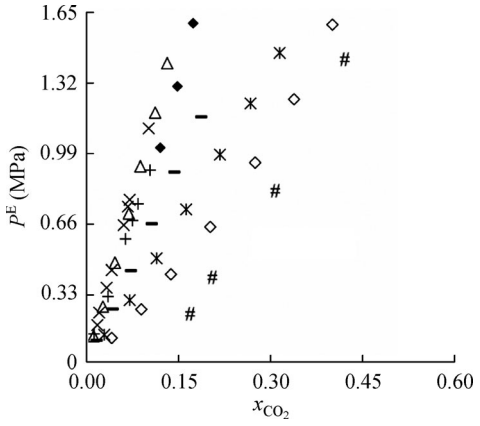

Fig. 6 CO_2 solubility in TTTM compared to that in ILs at 303.15 K. Symbols are: (♦) TTTM in this work; (#) [THTDP][NTf_2] (Carvalho et al., 2010); (×) [C_6mim][BF_4] (Shokouhi et al., 2010); (–) [C_6mim][OTf] (Jalili et al., 2010b); (+) [C_6mim][PF_6] (Jalili et al., 2010b); (*) [C_8mim][PF_6] (Safavi et al., 2013); (Δ) [C_2mim][$EtSO_4$] (Jalili et al., 2010a), and (◇) [C_8mim][NTf_2] (Jalili et al., 2012).

CO_2 capture performance due to the larger $|\Delta E|$ value. Therefore, $|\Delta E|$ data help us judge the ability of TTM and TTTM to capture CO_2. The $|\Delta E|$ values are listed in Table 7. As presented in this table, the second geometries of TTM (II) and TTTM (II) were almost stable than their first geometries (II). However, the first geometries were used to investigate CO_2 absorption. Because the main purpose of this study was how adding amine as a third part could increase CO_2 absorption. The optimized structures of second geometries are shown in Fig. S8 in Supplementary Material. From the data in Table 7, the $|\Delta E|$ value for TTTM (I) + CO_2 system was larger than that of TTM (I) + CO_2. Therefore, higher CO_2 affinity can be obtained by adding AMPD to a binary mixture of K_2CO_3 + EG, which was investigated by experimental CO_2 measurement in this work. Besides, the sums of van der Waals (vdW) atomic radii of H and O (2.5 Å) and H and N (2.6 Å) are considered as infallible indicators of H−bonding formation. Regarding the TTM (I) + CO_2 complex, no H-bond is developed between the solvent and CO_2. But a $107C_{CO_2}\cdots 2O_{CO_3}^-$ interaction with a bond distance of 2.84 Å and a $6K^+\cdots 108O_{CO_2}$ with a bond distance of 3.03 Å are formed. Upon AMPD addition to TTM, the new solvent (TTTM), is capable of developing $N\text{-}119H_{AMPD}\cdots 126O_{CO_2}$ H-bond with a bond distance of 2.37 Å. Two main interactions occurred between EG and CO_2, $23H_{EG}\cdots 127O_{CO_2}$, $60H_{EG}\cdots 127O_{CO_2}$ and $63H_{EG}\cdots 126O_{CO_2}$ with bond distances of 2.68 Å, 2.65 Å and 2.58 Å, respectively as well as a $125C_{CO_2}\cdots 121O_{AMPD}$ interaction with a bond distance of 3.09 Å. However, in the new solvent, the $6K^+\cdots 127O_{CO_2}$ distance increases to 4.03 Å. Therefore, the existing amine group in AMPD plays an important role in increasing CO_2 solubility in TTTM. The DFT analyses indicate good agreement with the results obtained from the experimental CO_2 solubility measurements.

4 Conclusions

In this work, two types of potassium carbonate-based transition-temperature mixtures were prepared. The binary transition-temperature mixture (TTM) was a combination of potassium carbonate HBA and EG HBD with a molar ratio of 1:10 HBA/HBD. To improve CO_2 solubility, a hindered amine, 2-amino-2-methyl-1,3-propanediol (AMPD), as another HBD was added to the TTM to

Table 6 The CO_2 solubility comparison between solvents in this work and TTMs/DESs in literature.

Solvent	T (K)	P^E (MPa)	x_{CO_2}	Ref.
DES				
Choline chloride /Urea (1:2.5)	313–333	1.06–12.55	0.032–0.203	Li et al., 2008
Choline chloride Ethanol amine (1:6)	298	1.0	0.11	Ali et al., 2014
Choline chloride /Diethanol amine (1:6)	298	1.0	0.0925	Ali et al., 2014
Choline chloride /Triethylene Glycol (1:6)	298	1.0	0.0419	Ali et al., 2014
Choline chloride /Glycerol (1:3)	298	1.0	0.0454	Ali et al., 2014
Methyltriphenylphosphonium Bromide/ Ethanol amine (1:6)	298	1.0	0.1441	Ali et al., 2014
Tetrabutylammonium Bromide/ Diethanol Amin (1:6)	298	1.0	0.0830	Ali et al., 2014
TTM				
Choline chloride /Latic acid (1:2)	303–348	0.83–9.38	0.248–0.0995	Francisco et al., 2013
Tetramethylammonium chloride/ Latic acid (1:2)	308	0.8–2.0	0.025–0.059	Zubeir et al., 2014
Tetraethylammoniumchloride/ Latic acid (1:2)	308	0.8–2.0	0.031–0.073	Zubeir et al., 2014
Tetrabutylammonium chloride/ Latic acid (1:2)	308	0.8–2.0	0.053–0.127	Zubeir et al., 2014
K_2CO_3/EG (1:10): TTM	303	1.080–1.794	0.1013–0.1697	This work
K_2CO_3/EG/AMPD (1:10:1): TTTM	303	1.010–1.780	0.1203–0.2022	This work

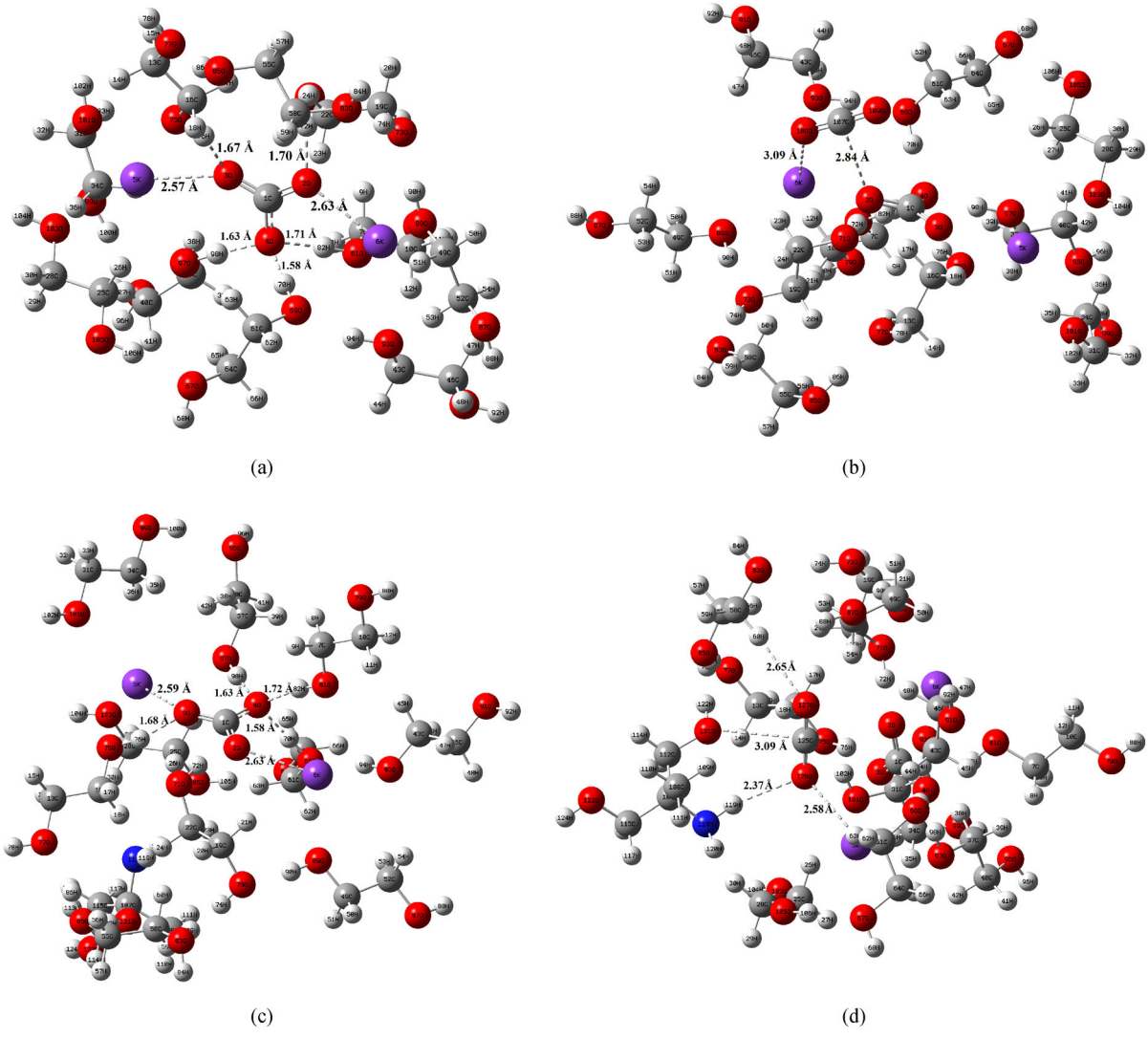

Fig. 7 Optimized structures of (a) TTM (l), (b) TTM (l)+ CO_2, (c) TTTM (l), (d) TTTM (l)+ CO_2 at the B3LYP/6-31 + G (d, p) level. Atom color code: (gray) carbon, (light gray) hydrogen, (red) oxygen, (purple) potassium, and (blue) nitrogen.

Table 7 Absoluteinteraction energy (|Δ*E*|) of systems with or without CO_2

System	|Δ*E*| (kJ/mol)
K_2CO_3	1507.78
TTM (l)	541.42
TTM (ll)	565.05
TTM (l) + CO_2	561.93
TTTM (l)	558.82
TTTM (ll)	598.60
TTTM (l) + CO_2	596.36

prepare a ternary transition-temperature mixture (TTTM). The main functional groups such as aliphatic (-CH_n), hydroxyl (-OH), amino (-NH_2), and the carbonate ion (CO_3^{-2}) were identified and analyzed by FT-IR. The results obtained by the spectra of both solvents confirmed that these solvents exhibit similar behavior to their HBDs, especially ethylene glycol. Although both TTM and TTTM showed similar spectra, their difference was in two peaks. In fact, there were two peaks in the spectra of TTTM which did not appear in the spectra of TTM. These peaks are an indication of the existence of the amino-functional group (-NH_2) on the structure of TTTM. The results showed that by adding AMPD to the binary mixture, the thermal stability and viscosity of TTTM increases compared to TTM. By employing Eyring's absolute rate theory, positive values of ΔH^* and ΔS^* were obtained for both solvents. Finally, CO_2 absorption was improved by adding AMPD to the mixture. The CO_2 solubility in TTTM was higher than that in TTM because of an additional amine functional group (-NH_2) in its structure. This was confirmed by DFT analysis by computing the interaction energy (|Δ*E* |) of systems. It was found that TTTM + CO_2 system has a

higher $|\Delta E|$ |value than the TTM + CO_2 system and amine group in AMPD of TTTM played an important role in the formation of H-bond between N-H_{AMPD}…O_{CO_2} resulting in higher CO_2 solubility in TTTM.

Acknowledgements Hosein Ghaedi and Ming Zhao are grateful for the support of National Key Research and Development Program of China (Grant No. 2019YFC1904602) and the Key SCI-Tech Innovation 2025 Program of Ningbo, China (Grant No. 2018B10025).

Electronic Supplementary Material Supplementary material is available in the online version of this article at https://doi.org/10.1007/s11783-021-1500-9 and is accessible for authorized users.

References

Abbas Q, Binder L (2010). Synthesis and characterization of choline chloride based binary mixtures. ECS Transactions, 33(7): 49–59

Ali E, Hadj-Kali M K, Mulyono S, Alnashef I, Fakeeha A, Mjalli F, Hayyan A (2014). Solubility of CO_2 in deep eutectic solvents: Experiments and modelling using the Peng–Robinson equation of state. Chemical Engineering Research & Design, 92(10): 1898–1906

Altamash T, Atilhan M, Aliyan A, Ullah R, García G, Aparicio S (2016). Insights into choline chloride–phenylacetic acid deep eutectic solvent for CO_2 absorption. RSC Advances, 6(110): 109201–109210

Borhani T N G, Azarpour A, Akbari V, Wan Alwi S R, Manan Z A (2015). CO_2 capture with potassium carbonate solutions: A state-of-the-art review. International Journal of Greenhouse Gas Control, 41: 142–162

Carvalho P J, Álvarez V H, Marrucho I M, Aznar M, Coutinho J A P (2010). High carbon dioxide solubilities in trihexyltetradecylphosphonium-based ionic liquids. Journal of Supercritical Fluids, 52(3): 258–265

Chemat F, Anjum H, Shariff A M, Kumar P, Murugesan T (2016). Thermal and physical properties of (Choline chloride + urea + l-arginine) deep eutectic solvents. Journal of Molecular Liquids, 218: 301–308

Francisco M, van den Bruinhorst A, Zubeir L F, Peters C J, Kroon M C (2013). A new low transition temperature mixture (LTTM) formed by choline chloride + lactic acid: Characterization as solvent for CO_2 capture. Fluid Phase Equilibria, 340: 77–84

García G, Atilhan M, Aparicio S (2015). A theoretical study on mitigation of CO_2 through advanced deep eutectic solvents. International Journal of Greenhouse Gas Control, 39: 62–73

Ghaedi H, Ayoub M, Sufian S, Hailegiorgis S M, Murshid G, Farrukh S, Khan S N (2017a). Experimental and prediction of volumetric properties of aqueous solution of (allyltriphenylPhosphonium bromide—Triethylene glycol) deep eutectic solvents. Thermochimica Acta, 657: 123–133

Ghaedi H, Ayoub M, Sufian S, Hailegiorgis S M, Murshid G, Khan S N (2018a). Thermal stability analysis, experimental conductivity and pH of phosphonium-based deep eutectic solvents and their prediction by a new empirical equation. Journal of Chemical Thermodynamics, 116: 50–60

Ghaedi H, Ayoub M, Sufian S, Lal B, Shariff A M (2017b). Measurement and correlation of physicochemical properties of phosphonium-based deep eutectic solvents at several temperatures (293.15 K to 343.15 K) for CO_2 capture. Journal of Chemical Thermodynamics, 113: 41–51

Ghaedi H, Ayoub M, Sufian S, Lal B, Uemura Y (2017c). Thermal stability and FT-IR analysis of Phosphonium-based deep eutectic solvents with different hydrogen bond donors. Journal of Molecular Liquids, 242: 395–403

Ghaedi H, Ayoub M, Sufian S, Murshid G, Farrukh S, Shariff A M (2017d). Investigation of various process parameters on the solubility of carbon dioxide in phosphonium-based deep eutectic solvents and their aqueous mixtures: Experimental and modeling. International Journal of Greenhouse Gas Control, 66: 147–158

Ghaedi H, Ayoub M, Sufian S, Shariff A M, Hailegiorgis S M, Khan S N (2017e). CO_2 capture with the help of Phosphonium-based deep eutectic solvents. Journal of Molecular Liquids, 243: 564–571

Ghaedi H, Ayoub M, Sufian S, Shariff A M, Lal B (2017f). The study on temperature dependence of viscosity and surface tension of several phosphonium-based deep eutectic solvents. Journal of Molecular Liquids, 241: 500–510

Ghaedi H, Ayoub M, Sufian S, Shariff A M, Lal B, Wilfred C D (2018b). Density and refractive index measurements of transition-temperature mixture (deep eutectic analogues) based on potassium carbonate with dual hydrogen bond donors for CO_2 capture. Journal of Chemical Thermodynamics, 118: 147–158

Ghaedi H, Ayoub M, Sufian S, Shariff A M, Murshid G, Hailegiorgis S M, Khan S N (2017g). Density, excess and limiting properties of (water and deep eutectic solvent) systems at temperatures from 293.15 K to 343.15 K. Journal of Molecular Liquids, 248: 378–390

Ghaedi H, Zhao M, Ayoub M, Zahraa D, Shariff A M, Inayat A (2019). Preparation and characterization of amine (N-methyl diethanolamine)-based transition temperature mixtures (deep eutectic analogues solvents). Journal of Chemical Thermodynamics, 137: 108–118

Guo W, Hou Y, Ren S, Tian S, Wu W (2013). Formation of deep eutectic solvents by phenols and choline chloride and their physical properties. Journal of Chemical & Engineering Data, 58(4): 866–872

Gutierrez M C, Carriazo D, Ania C O, Parra J B, Ferrer M L, del Monte F (2011). Deep eutectic solvents as both precursors and structure directing agents in the synthesis of nitrogen doped hierarchical carbons highly suitable for CO_2 capture. Energy & Environmental Science, 4(9): 3535–3544

Hayyan M, Hashim M A, Hayyan A, Al-Saadi M A, AlNashef I M, Mirghani M E S, Saheed O K (2013). Are deep eutectic solvents benign or toxic? Chemosphere, 90(7): 2193–2195

Hu X, Cai M, Yang S, Sejas S A (2018). Air temperature feedback and its contribution to global warming. Science China. Earth Sciences, 61 (10): 1491–1509

Jalili A H, Mehdizadeh A, Shokouhi M, Ahmadi A N, Hosseini-Jenab M, Fateminassab F (2010a). Solubility and diffusion of CO_2 and H_2S in the ionic liquid 1-ethyl-3-methylimidazolium ethylsulfate. Journal of Chemical Thermodynamics, 42(10): 1298–1303

Jalili A H, Mehdizadeh A, Shokouhi M, Sakhaeinia H, Taghikhani V (2010b). Solubility of CO_2 in 1-(2-hydroxyethyl)-3-methylimidazolium ionic liquids with different anions. Journal of Chemical Thermodynamics, 42(6): 787–791

Jalili A H, Safavi M, Ghotbi C, Mehdizadeh A, Hosseini-Jenab M, Taghikhani V (2012). Solubility of CO_2, H_2S, and their mixture in the ionic liquid 1-octyl-3-methylimidazolium bis(trifluoromethyl)sulfonylimide.J Phys Chem B, 116(9): 2758–2774

Jiang W J, Zhang J B, Zou Y T, Peng H L, Huang K (2020). Manufacturing Acidities of hydrogen-bond donors in deep eutectic solvents for effective and reversible NH_3 capture. ACS Sustainable Chemistry & Engineering, 8(35): 13408–13417

Kalhor P, Ghandi K, Ashraf H, Yu Z (2021). The structural properties of a $ZnCl_2$-ethylene glycol binary system and the peculiarities at the eutectic composition. Phys Chem Chem Phys, 23(23): 13136–13147

Khan M F S, Wu J, Cheng C, Akbar M, Liu B, Liu C, Shen J, Xin Y (2020). Insight into fluorescence properties of 14 selected toxic single-ring aromatic compounds in water: Experimental and DFT study. Frontiers of Environmental Science & Engineering, 14(3): 42

Larkin P (2011). Infrared and raman spectroscopy: Principles and spectral interpretation. Elsevier, Waltham, USA

Li X, Hou M, Han B, Wang X, Zou L (2008). Solubility of CO_2 in a choline chloride + urea eutectic mixture. Journal of Chemical & Engineering Data, 53(2): 548–550

López-Salas N, Gutiérrez M C, Ania C O, Fierro J L G, Luisa Ferrer M, Monte F d (2014a). Efficient nitrogen-doping and structural control of hierarchical carbons using unconventional precursors in the form of deep eutectic solvents. Journal of Materials Chemistry. A, Materials for Energy and Sustainability, 2(41): 17387–17399

López-Salas N, Jardim E O, Silvestre-Albero A, Gutiérrez M C, Ferrer M L, Rodríguez-Reinoso F, Silvestre-Albero J, del Monte F (2014b). Use of eutectic mixtures for preparation of monolithic carbons with CO_2-adsorption and gas-separation capabilities. Langmuir, 30(41): 12220–12228

Mat Hussin S A, Varanusupakul P, Shahabuddin S, Yih Hui B, Mohamad S (2020). Synthesis and characterization of green menthol-based low transition temperature mixture with tunable thermophysical properties as hydrophobic low viscosity solvent. Journal of Molecular Liquids, 308: 113015

Morrison H G, Sun C C, Neervannan S (2009). Characterization of thermal behavior of deep eutectic solvents and their potential as drug solubilization vehicles. International Journal of Pharmaceutics, 378 (1–2): 136–139

Nawar A, Ghaedi H, Ali M, Zhao M, Iqbal N, Khan R (2019). Recycling waste-derived marble powder for CO_2 capture. Process Safety and Environmental Protection, 132: 214–225

Pachauri R K, Reisinger A 2007. Climate Change 2007: Synthesis Report. Geneva, Switzerland, p. 104

Safavi M, Ghotbi C, Taghikhani V, Jalili A H, Mehdizadeh A (2013). Study of the solubility of CO_2, H_2S and their mixture in the ionic liquid 1-octyl-3-methylimidazolium hexafluorophosphate: Experimental and modelling. Journal of Chemical Thermodynamics, 65: 220–232

Scripps Institution of Oceanography 2021. Concentration of CO_2. https://scripps.ucsd.edu/programs/keelingcurve/ (Accessed 24 August 2021).

Shokouhi M, Adibi M, Jalili A H, Hosseini-Jenab M, Mehdizadeh A (2010). Solubility and Diffusion of H_2S and CO_2 in the Ionic Liquid 1-(2-Hydroxyethyl)-3-methylimidazolium Tetrafluoroborate. Journal of Chemical & Engineering Data, 55(4): 1663–1668

United States Environmental Protection Agency 2014. Global Greenhouse Gas Emissions Data. https://www.epa.gov/ghgemissions/global-greenhouse-gas-emissions-data (Accessed 25 August 2021)

Vranes M, Dozic S, Djeric V, Gadzuric S (2012). Physicochemical characterization of 1-butyl-3-methylimidazolium and 1-butyl-1-methylpyrrolidinium Bis(trifluoromethylsulfonyl)imide. Journal of Chemical & Engineering Data, 57(4): 1072–1077

Wang X, Song C (2020). Carbon capture from flue gas and the atmosphere: A perspective. Frontiers in Energy Research, 8: 560849

Wen Q, Chen J X, Tang Y L, Wang J, Yang Z (2015). Assessing the toxicity and biodegradability of deep eutectic solvents. Chemosphere, 132: 63–69

Xie J, Yan N, Liu F, Qu Z, Yang S, Liu P (2014). CO_2 adsorption performance of ZIF-7 and its endurance in flue gas components. Frontiers of Environmental Science & Engineering, 8(2): 162–168

Xu G C, Ding J C, Han R Z, Dong J J, Ni Y (2016). Enhancing cellulose accessibility of corn stover by deep eutectic solvent pretreatment for butanol fermentation. Bioresource Technology, 203: 364–369

Yang C, Ma P, Jing F, Tang D (2003). Excess molar volumes, viscosities, and heat capacities for the mixtures of ethylene glycol + water from 273.15 K to 353.15 K. Journal of Chemical & Engineering Data, 48 (4): 836–840

Yang S, Fan X, Liu J, Zhao W, Hu B, Lu Q (2021). Mechanism insight into the formation of H_2S from thiophene pyrolysis: A theoretical study. Frontiers of Environmental Science & Engineering, 15(6): 120

Zubeir L F, Lacroix M H M, Kroon M C (2014). Low transition temperature mixtures as innovative and sustainable CO_2 capture solvents. J Phys Chem B, 118(49): 14429–14441